We are IntechOpen, the world's leading publisher of Open Access books Built by scientists, for scientists

6,900
Open access books available

186,000
International authors and editors

200M
Downloads

Our authors are among the

154
Countries delivered to

TOP 1%
most cited scientists

12.2%
Contributors from top 500 universities

CLARIVATE ANALYTICS
BOOK CITATION INDEX
INDEXED

WEB OF SCIENCE™

Selection of our books indexed in the Book Citation Index
in Web of Science™ Core Collection (BKCI)

Interested in publishing with us?
Contact book.department@intechopen.com

Numbers displayed above are based on latest data collected.
For more information visit www.intechopen.com

3

Detection of Tsunamis from Changes in Ocean Surface Roughness

Benjamin D. Hamlington[1], Oleg A. Godin[2,3]
Vladimir G. Irisov[2,4] and Robert R. Leben[1]
[1]Colorado Center for Astrodynamics Research, University of Colorado at Boulder
[2]Cooperative Institute for Research in Environmental Sciences
University of Colorado at Boulder
[3]NOAA Earth System Research Laboratory, Physical Sciences Division, Boulder
[4]ZelTechnology LLC, Boulder
USA

1. Introduction

The need for a reliable system for early tsunami detection and warning was made painfully clear by the over two hundred thousand lives lost to the tsunami generated by the 9.3 magnitude Sumatra-Andaman earthquake that swept across the Indian Ocean on 26 December 2004 (Stein & Okal, 2005; Lay et al., 2005; Titov et al., 2005). The tsunami claimed the lives of over 220,000 people and despite a lag of up to several hours between the earthquake and arrival of the tsunami in some locations, the majority of victims were given little or no warning of the impending threat. While tsunamis occur much more frequently in the Pacific Ocean and a tsunami warning system has been in place in the region for many years, no such system was in place in the Indian Ocean and the communications infrastructure was not adequate for issuing widespread warnings at the time of the Sumatra-Andaman tsunami.

An early and dependable assessment of a tsunami threat requires detection of the tsunami wave in the open ocean away from the shore (Lautenbacher, 2005; Levin & Nosov, 2005; Bernard et al., 2006; Schindele et al., 2008). In the open ocean, however, the wave amplitude of the tsunami is small (generally less than one meter) and it is only as it approaches the shore that the tsunami rapidly grows in amplitude. Given the expansiveness of the ocean, sensors capable of detecting the tsunami must have very broad coverage. In addition to detecting the tsunami early enough to provide adequate warning, the method of detection must be reliable with few false warnings. If coastal populations go to great lengths to move to safe areas only to find out later such an evacuation was unnecessary, they may be less likely to heed warnings in the future.

By complementing traditional seismic data and point measurements as provided by the Deep-Ocean Assessment and Reporting of Tsunamis (DART) buoys network (Gonzalez et al., 2005; Bernard et al., 2006), satellite observations of tsunami manifestations can potentially improve the accuracy and timeliness of tsunami forecasts (Levin & Nosov, 2005; Synolakis & Bernard, 2006; Geist et al., 2007; Wei et al., 2008; Behrens et al., 2008), increase

the lead time of tsunami warnings, decrease the probability of false alarms (Walker, 1996; Dudley and Lee, 1998; Godin et al., 2004; Nagai et al. 2007), and help avoid unnecessary evacuations (Dudley and Lee, 1998; Bernard et al., 2006).

Satellites have detected gravity waves induced by tsunamis in the ionosphere and the potential to use global positioning system satellites (GPS) for early tsunami detection is being explored (Artru et al., 2005; Occhipinti et al., 2006). Satellite altimeters have also sampled several tsunamis over the past two decades. The satellite altimetry sea surface height (SSH) measurements of the Sumatra-Andaman tsunami were used by a number of authors to study the properties of the tsunami, its propagation and scattering from the coastline as well as to improve characterization of the seismic source of the tsunami, and to verify numerical models (Fine et al., 2005; Kulikov et al., 2005; Smith et al., 2005; Song et al., 2005; Titov et al., 2005; Ablain et al., 2006; Hirata et al., 2006; Kumar et al., 2006; Fujii & Satake, 2007; Gower, 2007; Hayashi, 2008; Hoechner et al., 2008; Sladen & Hebert, 2008). Detection of earlier weaker tsunamis in less extensive satellite altimetry SSH records is discussed by Okal et al. (1999) and Zaichenko et al. (2005).

Although measurements of SSH can provide definitive detection of sufficiently large tsunamis, the spatial coverage and temporal resolution of satellite altimeters are not suitable for forming the basis of a system for the early detection of tsunamis. Satellite altimeters provide measurements only along their ground tracks and generally require ten days to obtain near global coverage. The chances are remote of actually observing a tsunami early enough to warn coastal inhabitants. Of the tsunami manifestations in the deep ocean, variations in ocean surface roughness are the most relevant and promising to detect tsunamis from space provided that these factors can be revealed by orbiting active (scatterometers) and passive (radiometers) scanning and microwave sensors, which have broad coverage of hundreds of kilometers across the satellite ground track.

Tsunami-induced variations in surface roughness away from the shore were first observed in visible light originating from a tsunami approaching Oahu in 1994 (Walker, 1996; Dudley and Lee, 1998). These variations were given the name "tsunami shadows" and appear as extended darker strips on the ocean surface along a tsunami front. Formation of the tsunami shadows as areas with a different root mean square (RMS) surface slope has been explained theoretically as a result of air-sea interaction; specifically tsunami-induced perturbations in the wind velocity close to the ocean surface that are predicted to be much larger than currents in the tsunami wave (Godin, 2003, 2004; Rowan, 2004). Later theoretical studies (Godin, 2005; Troitskaya & Ermakov, 2008) corroborated these conclusions.

The first definitive measurements of the tsunami effect on sea surface height and radar backscattering strength (a measure of ocean surface roughness) in the open ocean were obtained from satellite altimeters during passage of the 2004 Sumatra-Andaman tsunami. In this study we concurrently employ radar backscattering strength and SSH data obtained by satellite altimeters for the Sumatra-Andaman event as well as for three other tsunamis. Through statistical analyses of multiple years of satellite altimeter observations, we definitively demonstrate that the Sumatra-Andaman tsunami induced distinctive variations in ocean surface roughness and tentatively demonstrate that three other tsunami-induced variations in ocean surface roughness.

The sections below are organized as follows: In section 2, we outline a theory explaining the magnitude and spatial structure of tsunami-induced variations in ocean surface roughness. In section 3, we discuss our analysis of ocean surface roughness variations by introducing the data used in this study and explaining the statistical randomization tests. Section 4

provides results of the randomization tests for the 2004 Sumatra-Andaman tsunami as well as three other weaker tsunamis and demonstrates that the tsunami causes distinct, detectable changes in ocean surface roughness. In section 5, we discuss the feasibility of using variations in ocean surface roughness for the early detection of tsunami waves. Section 6 provides a summary and discussion of further research on this topic.

2. Theory of tsunami-induced wind velocity perturbations

Long surface gravity waves in the ocean modulate short gravity and gravity-capillary waves, and change ocean surface roughness through the interaction of short waves with near-surface currents and variations of near-surface wind-induced by long waves (Hara & Plant, 1994; Troitskaya, 1994; Kudryatsev et al., 1997; Cohen & Belcher, 1999; Godin & Irisov, 2003). Modulation due to currents is negligible for a tsunami in the deep ocean (Godin, 2003, 2004). Tsunami-induced variations in ocean surface roughness away from the shore result from variations in wind velocity that accompany tsunami waves, and have been predicted to be much larger than currents in the tsunami wave (Godin, 2003, 2004, 2005). Godin (2003, 2004, 2005) found that significant variations in the mean wind velocity arise from the generation of viscous waves in the atmosphere by coherent large-scale motion of the ocean surface in a tsunami wave. However, the magnitude of the surface roughness modulations and the position of areas with increased and decreased roughness are sensitive to the choice of a closure hypothesis for turbulence in the atmospheric boundary layer. Although any theoretical explanation of tsunami-induced surface roughness variations is still tentative, measuring these variations in the open ocean can provide insight into the physics of the interaction of fast surface waves with turbulent wind.

As outlined in Godin et al. (2009), there is no universally accepted model of airflow over fast sea waves. Using assumptions made in (Godin, 2005), in the presence of a monochromatic tsunami wave, the wind speed relative to the ocean surface retains a logarithmic profile up to a few tens of meters above the surface. The effective wind speed depends on characteristics of the tsunami and differs from the background wind speed by the factor:

$$M = 1 - \frac{\kappa a c}{H u_* \ln \beta} \tag{1}$$

where κ is the von Karman constant, u_* is the friction velocity, H is the height of the background logarithmic boundary layer, a is the SSH change due to the tsunami, c is the tsunami phase speed,

$$\beta = \frac{\kappa u_* T}{2\pi z_0} \tag{2}$$

z_0 is the roughness length, and T is the tsunami period.

For a monochromatic tsunami wave, the effective wind speed varies periodically in time with the SSH change. As long as the relaxation time of wind waves is much smaller than the tsunami period, the time dependence of the effective wind speed can be disregarded when determining characteristics of the ocean surface roughness that correspond to a given instantaneous value of the wind modulation M. Variations in the radar backscattering strength at nadir, σ_0, resulting from the tsunami-induced wind variations can be found in

the Modified Chelton-Wentz algorithm (Witter & Chelton, 1991) or the Freilich-Challenor algorithm (Freilich & Challenor, 1994) by comparing the σ_0 values that correspond to the background and effective wind speeds. In section 5, computed estimates of the maximum and minimum radar backscattering strength variations will be compared to measurements taken by the Jason-1 satellite altimeter during the 2004 Sumatra-Andaman tsunami.

3. Statistical analysis of ocean surface roughness variations

3.1 Data
Satellite altimetry provides concurrent measurements of SSH and σ_0. While not the focus of our study, SSH measurements allow us to identify the location of the leading edge of the tsunami. Detection of tsunamis in SSH measurements has been demonstrated in several previous studies (Okal et al., 1999; Ablain et al., 2006), although weak tsunamis generally remain obscured by background ocean variability. By utilizing satellite altimetry data, we are able to identify the location of the tsunami's leading edge in SSH measurements and test the concurrently measured σ_0 values for tsunami-induced changes in ocean surface roughness.

While initial studies have focused on the 2004 Sumatra-Andaman tsunami, the statistical analysis described below can be applied to any tsunami event occurring within the modern altimetry era. The Radar Altimeter Database System (RADS) was used to search and collect historical altimeter records. RADS allow the user to quickly search and obtain records from several satellite altimeters (Naeije et al., 2000). With the poor spatial coverage and temporal resolution provided by satellite altimeters, the chances of an altimeter sampling a tsunami are remote. Through an extensive search of the past 17 years of satellite altimetry data, we have identified four tsunami events on which we will focus our attention: 1992 Nicaraguan tsunami, 1995 Chile tsunami, 2004 Sumatra-Andaman tsunami, and 2010 Chile tsunami.

3.2 Statistical randomization tests
Ocean surface roughness is influenced by diverse phenomena in the ocean and atmosphere, including wind gusts, currents, internal gravity waves, and oceanographic fronts. The resulting σ_0 variability can far exceed the expected tsunami-induced variations. To determine whether the σ_0 variations observed were indeed caused by a tsunami and whether tsunami signals can be reliably extracted from σ_0 data, data with and without the tsunami present must be compared.

Tsunamis have several distinctive spatio-temporal characteristics that aid in the retrieval of the tsunami signal from the "noise" arising from other geophysical processes. Perhaps the most distinctive attribute of tsunami-induced roughness variations is their propagation speed relative to the ocean bottom. However, satellite altimeters only provide a "snapshot" of the ocean surface, and thus the propagation speed of the tsunami cannot be used to identify tsunami-induced features in satellite altimeter data. Instead, we systematically utilize spatial filtering (Powell & Leben, 2004) to suppress σ_0 variations that are unrelated to tsunamis.

To determine if σ_0 variations were induced by the passage of a tsunami, statistical randomization tests (Edgington, 1995) were performed to compare data with and without the tsunami present. One thousand 3.2°-windows (each containing 64 points of data) were randomly selected from the area of the ocean through which the tsunami passed. Mean σ_0 values were subtracted in each window to calculate the σ_0 anomaly. The RMS values and

the number of zero crossings were calculated for the σ_0 anomaly in each window and compared to the respective values in the 3.2°-window containing the leading edge of the tsunami. The RMS σ_0 anomaly characterizes the strength of the surface roughness variations, while the number of zero crossings serves as a measure of the spatial scale of the variations. If the tsunami-induced variations were distinctive and unique, we would expect the window containing the leading edge of the tsunami to have both a higher RMS and a greater number of zero crossings than found in the 1,000 randomly selected windows.

In addition to the randomization tests using the RMS σ_0 anomaly and zero crossings, a spectral approach is implemented. In each randomly selected 3.2°-window, the σ_0 and SSH data were detrended by removing the linear fit computed using least-squares. Windows with unphysically large SSH variations of more than 150 cm from the median were excluded if randomly selected. The Fourier spectrum of the detrended data was normalized to account for the high variability of the high-frequency part of the spectrum. The Fourier components with spatial scales from 90 km to 300 km, scales representative of the tsunami, were summed. To quantify the correlation between the σ_0 and SSH anomalies, the Fourier spectrum of their cross-correlation function was calculated in the range from 90 km to 300 km. The spectral measure of the σ_0 anomaly correlation with the SSH anomaly was computed for each of the 1,000 randomly selected windows and compared to the spectral measure computed for the window containing the leading edge of the tsunami. If the spectral measure of the window containing the tsunami signal is larger than the spectral measure computed for the randomly selected windows, we can determine that the σ_0 variations during the tsunami were unique and attributable to the passage of the tsunami.

4. Results

4.1 2004 Sumatra-Andaman tsunami

Four satellite altimeters overflew the 2004 Sumatra-Andaman tsunami during its propagation across the Indian Ocean. Envisat, Geosat Follow-On (GFO), Jason-1, and TOPEX/Poseidon measured the tsunami at times ranging from two hours to seven hours after the tsunamigenic earthquake occurred. Of these four satellite altimeters, Jason-1 provides the earliest observations of the Sumatra-Andaman tsunami and has the most extensive records. Jason-1 encountered the leading edge of the tsunami 1 h 53 minutes after the earthquake (Ablain et al., 2006; Gower, 2007) at about 5°S in the Indian Ocean heading northeast on ascending pass 129 of cycle 109 (Fig. 1). Since the satellite launch in 2001, Jason-1 has collected an extensive set of high-quality SSH and σ_0 data, allowing us to characterize the variability of the radar backscattering strength under various atmospheric conditions without the presence of the tsunami.

The leading front of the tsunami is contained in the window between 6°S and 2°S, with the spatial extent of the segment on the order of the tsunami wavelength. The tsunami signal is clearly present in this window and is well above the noise level in SSH records (Fig. 2A). Data quality in this window is high and there are few data points excluded by quality controls. Radar backscattering strengths measured in both the Ku- and C- microwave frequency bands in the vicinity of the leading front of the tsunami show up to 1 dB variations, which are not present in measurements along the same pass of the cycles before and after the tsunami (Fig. 2B, C). Using equations 1 and 2, and assuming the height of the background logarithmic boundary layer to be $H = 50-70$ m (Garratt, 1994), we calculate the
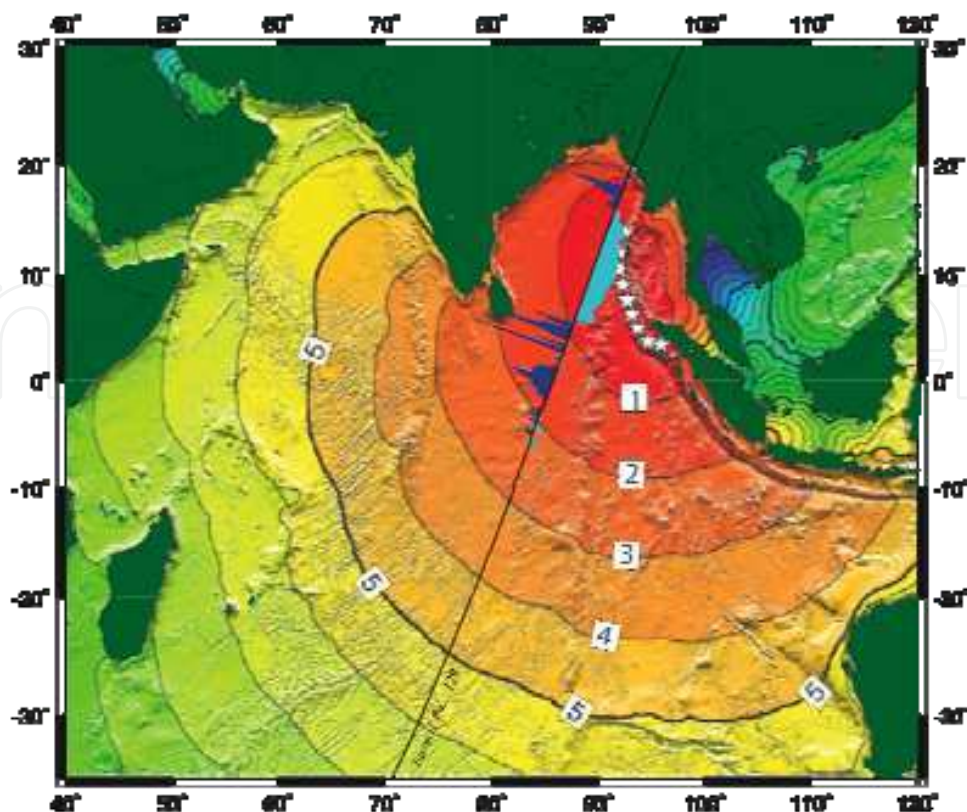
Fig. 1. Jason-1 satellite altimeter overflight of the Sumatra-Andaman tsunami. The Jason-1 ground track and C-band σ_0 data for pass 129 of cycle 109 is superimposed on contours of the tsunami leading wave front at hourly intervals after the earthquake. White stars show the location of the tsunami wave sources. (Tsunami wave front graphic is provided courtesy of the National Geophysical Data Center/ NOAA)

tsunami period to be T = 35-45 min (Gower, 2007), and a maximum and minimum SSH anomaly of 0.6-0.7m and –(0.4-0.5m). We obtain values of about 1 dB for the maximum variation of the radar backscattering strength that are consistent with the values in Figs. 2B and C. A more detailed comparison of the observed to predicted σ_0 variations, however, is not possible because of uncertainty in knowledge of the local meteorological parameters and the tsunami spectrum, and the high sensitivity of the tsunami-induced changes in the surface roughness to poorly known environmental parameters, such as the background wind speed. Despite this difficulty, the σ_0 variations can be attributed to the tsunami by performing statistical randomization tests using historical Jason-1 σ_0 data and comparing to the σ_0 data collected during the passage of the tsunami. The Jason-1 σ_0 data obtained during the Sumatra-Andaman tsunami passage were discussed by Troitskaya & Ermakov (2005; 2008), but they did not compare the data to analogous data in the absence of the tsunami.

To perform the randomization tests, one thousand 3.2°-windows centered between 20°S and 10°N were randomly selected in the tropical Indian Ocean from cycles 1-174 of Jason-1. The data were processed as outlined in section 3.2, and the RMS values and the number of zero crossings were calculated for the σ_0 data in each window and compared to the respective values in the window covering 5.6°S to 2.4°S along pass 129 of cycle 109. Only a few percent of the randomly selected windows simultaneously have equal or larger values of both the RMS σ_0 anomaly and the number of zero crossings. The statistical significance of the

hypothesis that surface roughness variations with and without the tsunami are not substantially different is 3.15% and 0.93% when estimated using the Ku- and C-band σ_0 data, respectively (Fig. 3).

As described in section 3.2, we also performed randomization tests implementing a spectral approach. Each 3.2°-window was processed and filtered as outlined in section 3.2, and the Fourier spectrums were computed for the σ_0 anomalies and cross-correlation function of the SSH and σ_0 anomalies. The spectral measures of these anomalies were compared to those computed for the window covering 5.6°S to 2.4°S along pass 129 of cycle 109. The probability distribution densities of the spatially filtered σ_0 anomaly, as measured in the C-band (Fig. 4a) and the σ_0 – SSH correlation (Fig. 4b), show that the σ_0 variability equalled or exceeded its level in the tsunami event in 1.7% of the cases, while the correlation level in the tsunami event was uniquely large. For the σ_0 data obtained in the Ku-band, the corresponding significance level is 6.8% for the σ_0 variability (Fig. 4c); the σ_0 – SSH correlation remains uniquely large in the tsunami event (Fig. 4d). Thus, the randomization tests provide strong support for the hypothesis that the σ_0 variations and hence the underlying surface roughness variations observed by Jason-1 during the passage of the Sumatra-Andaman tsunami passage, were caused by the tsunami.

In addition to detecting the leading wave front of the tsunami where the amplitude of the wave is often the largest, it is important to be able to detect the tsunami away from
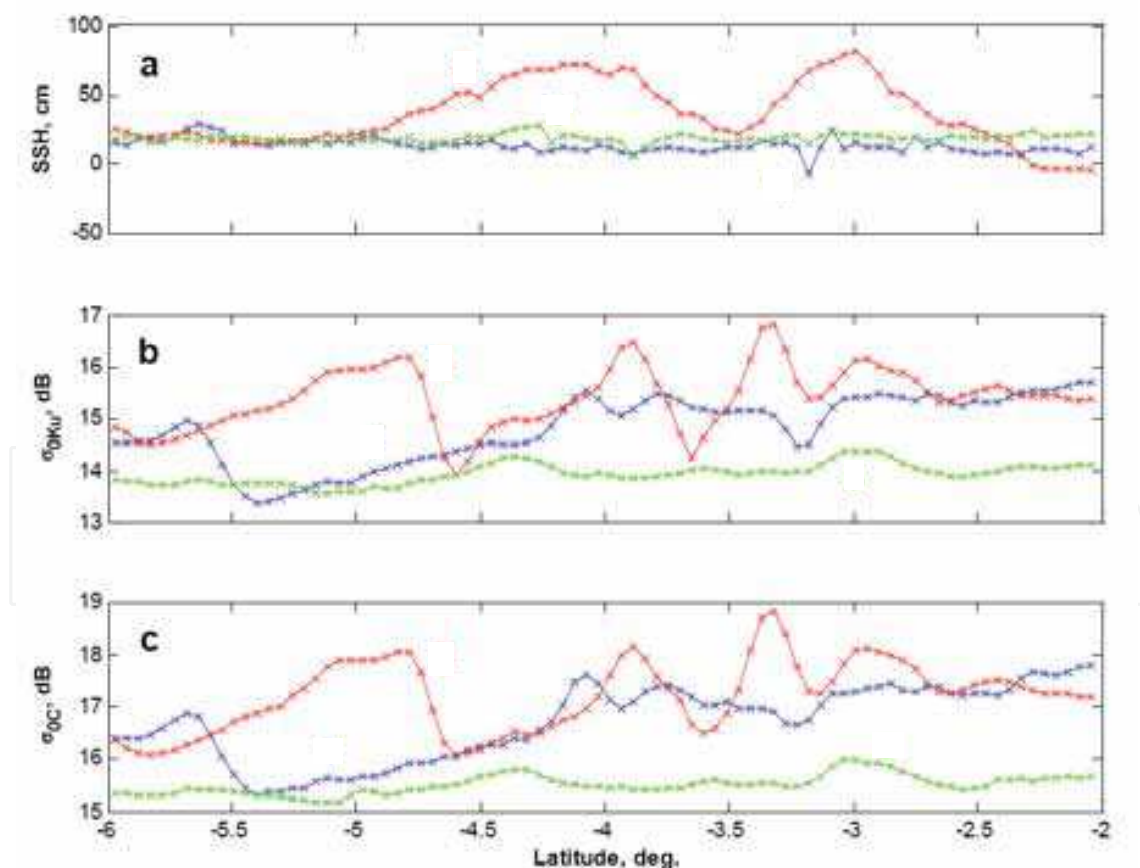

Fig. 2. Jason-1 data for pass 129 from 6°S to 2°S shown for the cycles before the tsunami (blue), coincident with the tsunami (red) and after the tsunami (green). (a) Sea surface height. (b) Ku-band radar backscattering strength. (c) C-band radar backscattering strength
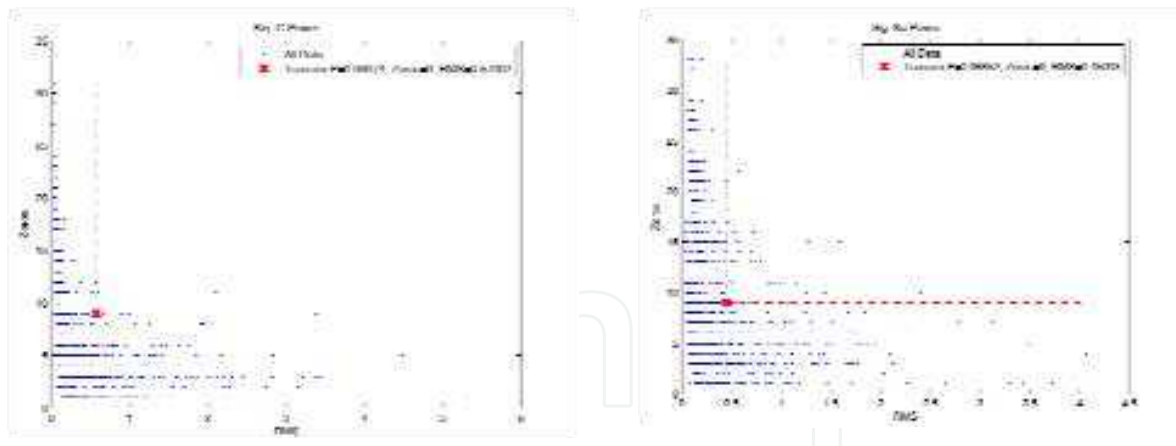
Fig. 3. Randomization tests of the radar backscattering strength data. (a) Ku-band σ_0 data. (b) C-band σ_0 data. Statistical significance of the hypothesis that surface roughness variations with and without the tsunami are not substantially different is found to be 3.15% and 0.93% for the Ku-band and C-band measurements respectively

the leading edge where the magnitude of the tsunami has been diminished. We applied the same data processing techniques to 3.2° non-overlapping windows, which extend from 2.4°S (where the window test above ends) to the north along the Jason-1 pass 129 of cycle 109. Windows that contained data gaps too extensive to apply the processing and filtering techniques were excluded from the subsequent randomization tests. The other two windows that were used for testing ranged from 2.5°S to 0.7°N and from 0.8°N to 4.0°N. For the window beginning at 2.5°S, only 9.1% and 9.7% of the randomly selected windows simultaneously have equal or larger numbers of both RMS σ_0 anomalies and the number of zero crossings in the Ku- and C-bands, respectively. For the window beginning at 4.0°N, only 6.4% and 2.2% of the randomly selected windows had greater RMS σ_0 anomaly and more zero crossings for the Ku- and C-bands, respectively. Similarly, for the randomization test using the spectral approach, the window beginning at 2.5°S yielded a spectral measure for the $\sigma_0 - SSH$ correlation that was uniquely large. The same analysis could not be applied to the window beginning at 0.8°N due to data gaps.

These additional randomization tests away from the leading wave front of the tsunami reinforce the evidence of exceptional features in radar backscattering strength in the presence of a tsunami. Furthermore, these results demonstrate that our data processing algorithms allow detection of the tsunami manifestations in the radar backscattering strength for various tsunami waveforms and can successfully discriminate between regions where the tsunami is and is not present.

4.2 2010 Chile tsunami

Detection of tsunami manifestations in the Jason-1 σ_0 records was simplified by the extraordinary strength of the Sumatra-Andaman tsunami. Other weaker tsunamis provide a much more rigorous test of our detection algorithm. As a result of excellent satellite altimeter coverage, a good candidate for analysis is the 2010 Chile tsunami that was generated by an Mw 8.8 earthquake on February 27th, 2010. Tsunami waves hit coastal towns in Chile with substantial wave heights. Although a warning was generated for the entire Pacific region, the tsunami did not significantly affect other areas such as Hawaii, New Zealand, Australia, or Japan. There were multiple satellite altimeters (Jason-1, Jason-2
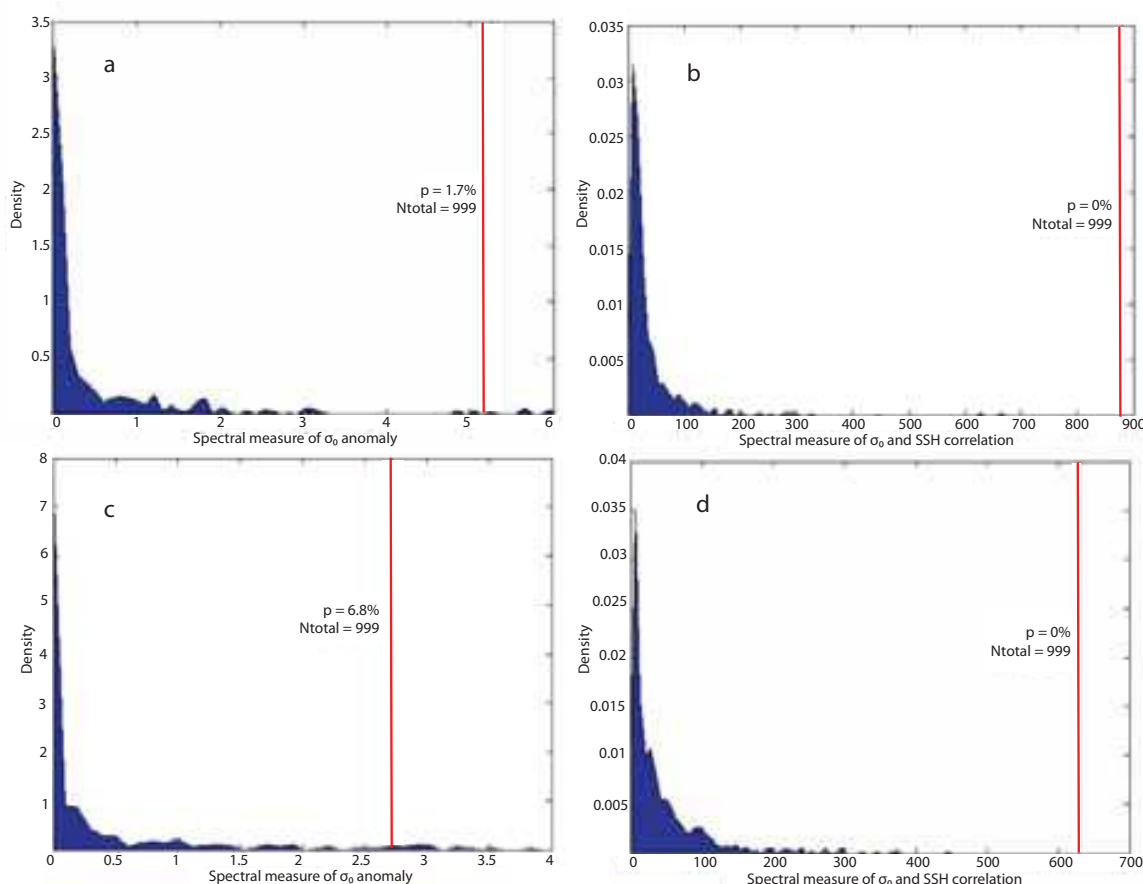
Fig. 4. Randomization tests of the spectral measures of the radar backscattering strength anomaly and its correlation with sea surface height anomaly as observed by Jason-1 in the vicinity of the tsunami leading front. (a) Randomization tests of the spatially filtered C-band σ_0 anomaly. (b) Randomization tests of the co-spectrum of the spatially filtered C-band σ_0 and sea surface height anomalies. (c) Randomization tests of the spatially filtered Ku-band σ_0 anomaly. (d) Randomization tests of the co-spectrum of the spatially filtered Ku-band σ_0 and sea surface height anomalies

and Envisat) that overflew the tsunami wave field shortly after the earthquake occurred. Resulting largely from the weak tsunami and small wave amplitude in the open ocean, the tsunami signal was only definitively identified in one pass from these three altimeters despite the excellent altimeter coverage. Using a simple filtering technique to remove variations in SSH not resulting from the tsunami, the leading wave front of the tsunami is positively identified about 7.5 hours after the generation of the tsunami in pass 143 of Jason-1 cycle 300 around 15°S. The passes from the cycles 299 and 301 (before and after the one coincident with the tsunami) were averaged together, smoothed and then subtracted from pass 143 of Jason-1 cycle 300. The filtered signal agrees reasonably well with the Method of Splitting Tsunami (MOST) model results obtained from NOAA/ PMEL/ Center for Tsunami Research (Synolakis et al., 2008) for the Chile tsunami, and confirms the location of the leading edge near 15°S (Fig. 5). The spatial extent of the leading edge, however, differs between the filtered Jason-1 signal and the results from the MOST model, likely resulting from the oblique sampling of the tsunami by Jason-1. In other words, the Jason-1 ground track of pass 143 did not enter very far into the tsunami wave field and stayed close to the leading front of the tsunami as the wave propagated across the Pacific Ocean. Fig. 6A shows
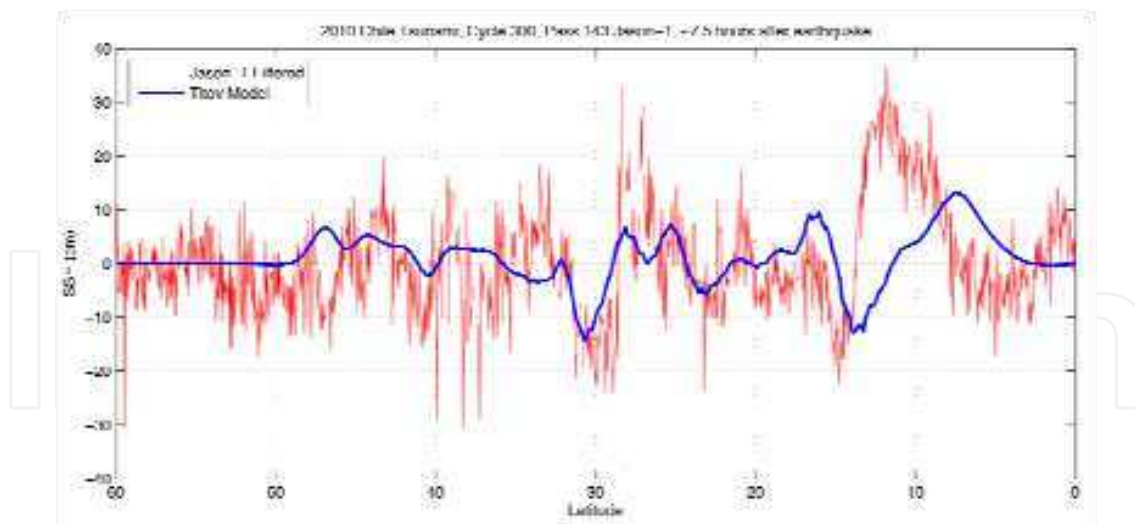
Fig. 5. Filtered SSH data from pass 143 of cycle 300 of Jason-1, occurring about 7.5 hours after the earthquake. The filtered signal is in agreement with the results from the MOST model and appears to confirm the location of the leading wave front of the tsunami around 15°S

the MOST model results at the time Jason-1 entered the tsunami wave field, while Fig. 6B shows the model results at the time the satellite altimeter departed the tsunami wave field. As a result of the oblique sampling of Jason-1, a small time difference between reality and model could result in a considerable change in the location and spatial extent of the leading edge of the tsunami.

The leading front of the tsunami is contained in the window between 16°S and 12°S, with the spatial extent of the segment on the order of the tsunami wavelength. The tsunami signal is clearly present in this window with amplitude of greater than 20 cm (Fig. 5 & 7A). Data quality in this window is high and there are few data points excluded by quality controls. Radar backscattering strengths measured in both the Ku and C microwave frequency bands in the vicinity of the leading front of the tsunami do not show variations as strong as those observed for the 2004 Sumatra-Andaman tsunami, particularly in the C-band. This is not surprising given the relative strengths of the two tsunamis.

To perform the randomization tests, one thousand 3.2° windows centered between 50°S and 10°N were randomly selected in the Pacific Ocean from cycles 1-305 of Jason-1. The data was processed as outlined in section 3.2, and the RMS values and the number of zero crossings were calculated for the σ_0 data in each window and compared to the respective values in the window covering 15.5°S to 12.3°S along pass 143 of cycle 300. The statistical significance of the hypothesis that the surface roughness variations with and without the tsunami are not substantially different is 0.4% and 20.8% when estimated using the Ku- and C-band σ_0 data, respectively. While the randomization test on the Ku-band radar backscattering strength yielded positive identification at the 1% significance level, 30 zero crossings and an RMS σ_0 anomaly of only 0.20 were found for the window containing the leading front of the tsunami. The high significance level obtained from the randomization test is primarily a result of the large number of zero crossings. Given the physical characteristics of the tsunami, we would expect fewer zero crossings. Without knowledge of the wind speed at the time of the tsunami, however, the expected RMS σ_0 anomaly is unknown. The C-band radar backscattering strength for the same window contained 10 zero
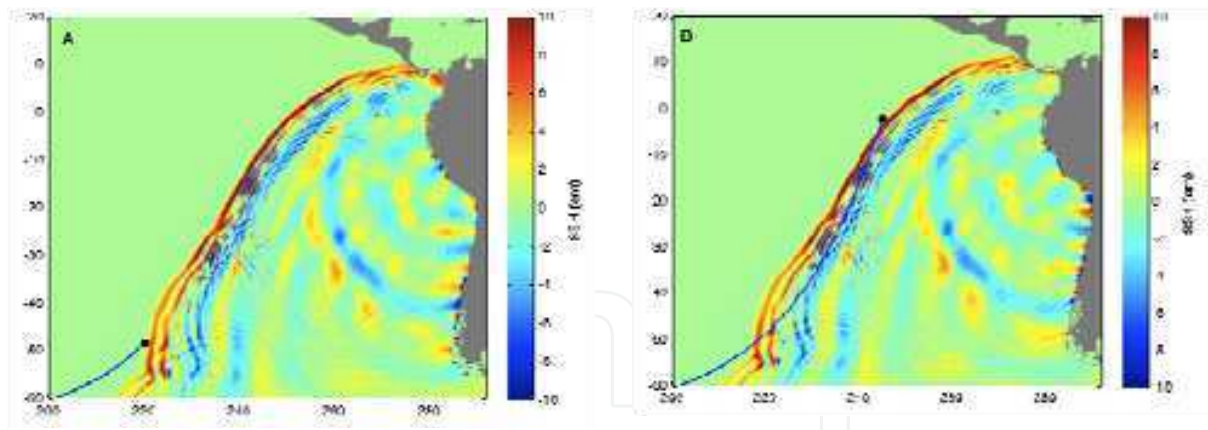
Fig. 6. MOST model results at the time Jason-1 entered the tsunami wave field (according to the model) (A) and at the time Jason-1 departed the tsunami wave field (B). The oblique sampling of the leading front of the tsunami by Jason-1 provides a possible explanation for the discrepancy between model results and Jason-1 data as seen in Fig. 5
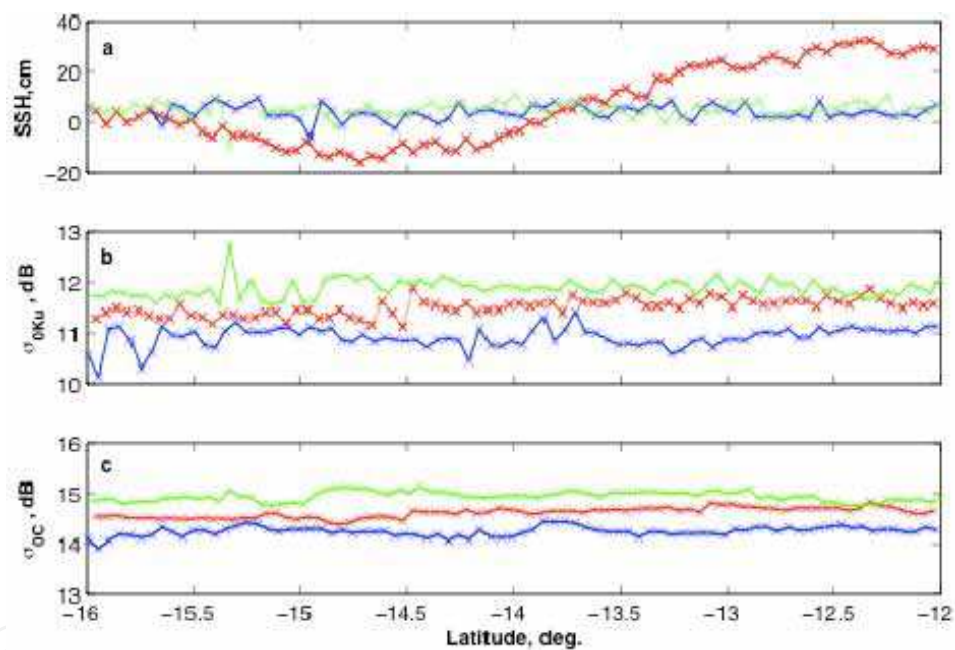

Fig. 7. Jason-1 data for pass 143 from 16°S to 12°S shown for the cycles before the 2010 Chile tsunami (blue), coincident with the tsunami (red) and after the tsunami (green). (a) Sea surface height. (b) Ku-band radar backscattering strength. (c) C-band radar backscattering strength

crossings and RMS σ_0 anomaly of 0.12, producing poor results for the randomization tests. The randomization tests utilizing the spectral approach were not conducted because the lack of noticeable variations in the σ_0 anomaly and weaker SSH anomaly signal are unlikely to produce positive results.

4.3 1992 Nicaragua tsunami and 1995 Chile tsunami
While we have positively detected the tsunami-induced variations in ocean surface roughness for the 2004 Sumatra-Andaman tsunami, we have only tentatively identified the

tsunami-induced variations for the 2010 Chile tsunami, raising questions about the ability to detect weaker tsunami signals. Okal et al. (1999) studied seven other tsunami events using satellite altimetry. Using only SSH measurements, one tsunami (1992 Nicaragua Tsunami) was positively detected and another tsunami (1995 Chile tsunami) was tentatively detected. Using the statistical randomization tests, we can attempt to detect the tsunami-induced variations in ocean surface roughness.

The 1992 Nicaragua tsunami was generated by a "tsunami earthquake," i.e., an earthquake that produces an unusually large tsunami relative to the earthquake magnitude due to a slow rupture (Kanamori & Kikuchi, 1972). The ERS-1 satellite altimeter sampled the tsunami wave field on passes 523 and 525 of cycle 87. Both tracks sampled the tsunami about 3.5 and 5.5 hours after the tsunamigenic earthquake, respectively. Okal et al. (1999) determined that the tsunami signal could not be detected in pass 523 and focused their attention on 525. ERS-1 entered the tsunami wave field around 17°S, with wave amplitudes seen in the SSH of less than 10 cm (Fig. 8). Variations in the radar backscattering strength were around 0.5 dB.

To perform the randomization tests, one thousand 3.2° windows between 40°S and 20°N were randomly selected in the Pacific Ocean from cycles 83-101 of ERS-1. The data was processed as outlined in section 3.2, and the RMS values and the number of zero crossings were calculated for the σ_0 data within each window and compared to the respective values in the window covering 17.0°S to 13.8°S along pass 525 of cycle 87. The statistical significance of the hypothesis that the surface roughness variations with and without the tsunami are not substantially different is 2.6% when estimated using the Ku-band σ_0 data. This suggests a positive identification of the tsunami signal from variations in ocean surface roughness.

As mentioned above, Okal et al. (1999) tentatively identified the 1995 Chile tsunami from SSH measurements. A relatively large earthquake generated a tsunami with run-ups of 2 m in the Marquesas Islands. The TOPEX/ Poseidon satellite altimeter sampled the tsunami wave field along two passes (230 and 232) of cycle 105, 3 and 5 hours after the earthquake occurred. The tsunami signal was not detected in pass 230, but there was tentative identification of the tsunami in pass 232. Okal et al. (1999) estimate that TOPEX/ Poseidon entered the tsunami wave field around 36°S and exited the wave field around 25°S. SSH wave amplitudes in this region were found to be only 10 cm with maximum variations in the radar backscattering strength of approximately 0.4 dB (Fig. 9). Additionally, comparing the SSH data from the cycles before and after the one coincident with the tsunami show very little variation in SSH from cycle to cycle. When using these cycles to filter the target cycle, only a small signal with amplitude of much less than 10 cm remains near 27°S (Fig. 10).

We performed the randomization tests by randomly selecting one thousand 3.2°-windows centered between 50°S and 10°N in the Pacific Ocean from cycles 50-200 TOPEX/ Posedion. The data was processed as outlined in section 3.2, and the RMS values and the number of zero crossings were calculated for the σ_0 data in each window and compared to the respective values in the window covering 29.0°S to 25.8°S along pass 232 of cycle 105. The statistical significance of the hypothesis that the surface roughness variations with and without the tsunami are not substantially different is 2.5% when estimated using the Ku-band σ_0 data. This suggests a positive identification of the tsunami signal from the variations in ocean surface roughness. Given the relatively small signal found in the SSH data, however, this identification remains tentative.
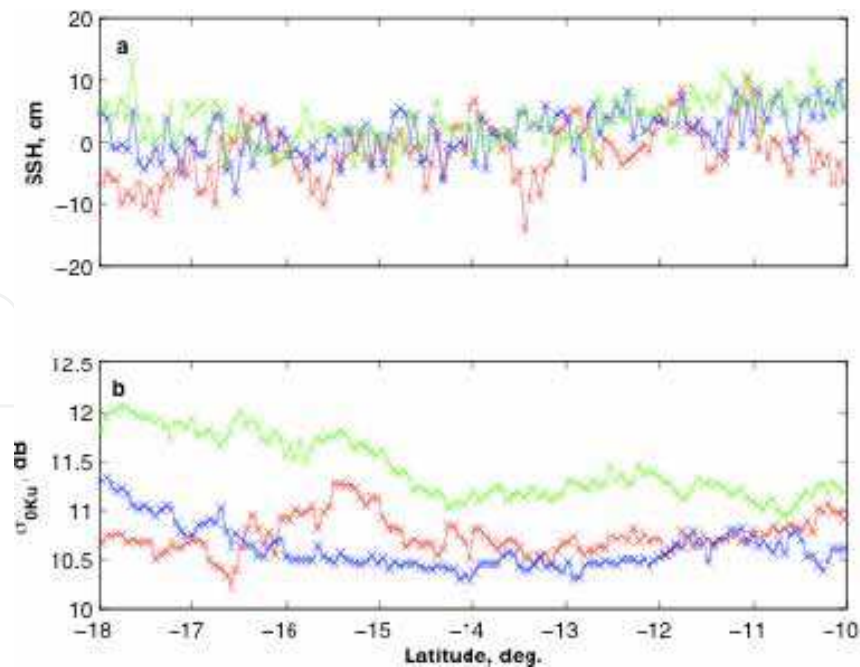
Fig. 8. ERS-1 data for pass 525 from 18°S to 10°S shown for the cycles before the 1992 Nicaragua tsunami (blue), coincident with the tsunami (red), and after the tsunami (green). (a) Sea surface height. (b) Ku-band radar backscattering strength

5. Feasibility of tsunami early detection and warning

The use of radar backscattering strength measurements for the detection of a tsunami in the open ocean has been positively demonstrated for the 2004 Sumatra-Andaman tsunami and tentatively demonstrated for the 1992 Nicaragua tsunami, 1995 Chile tsunami, and 2010 Chile tsunami. Satellite altimeters provide concurrent measurements of SSH and σ_0 allowing for the identification of the leading edge in SSH and subsequent testing of this leading edge using randomization tests on σ_0 measurements. While the four tsunamis mentioned above were well sampled by satellite altimeters, historically satellite altimeter measurements of tsunamis are uncommon. Even with several satellites on orbit, nadir-pointing satellite altimeters do not provide the ground track coverage necessary to ensure sampling of a tsunami wave field. Furthermore, as the results above show, even if timely sampling of the tsunami was available in real time, separating the tsunami signal from the background ocean variability is difficult. The use of satellite altimeters as the foundation for an early detection system is not plausible.

While radar backscattering measurements from satellite altimeters are only available along one-dimensional lines traced by the nadir ground track, two-dimensional images of tsunami-induced changes in ocean surface roughness could be obtained by using microwave radiometers and radars already on orbit. As outlined in section 2, Godin et al. (2009) present a model for calculating the tsunami-induced changes in ocean surface roughness, providing a factor directly related to SSH that corresponds to the modulation of background wind speed resulting from the passage of a tsunami. The ability to detect the tsunami from such a two-dimensional image is largely dependent on the variability and strength of the background wind field at the time of the tsunami passage. With a constant background wind of physically realistic magnitude, the tsunami-induced changes in ocean
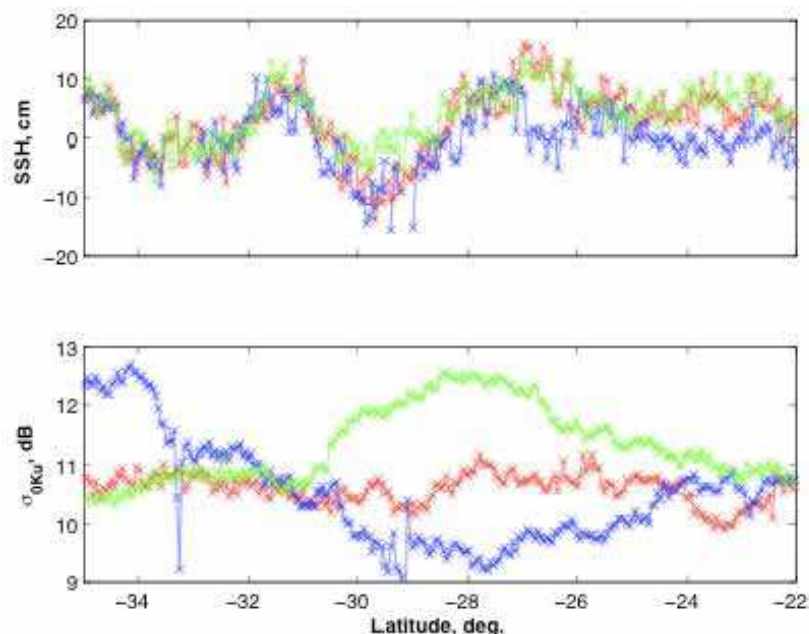
Fig. 9. TOPEX/ Posedion data for pass 232 from 35°S to 22°S shown for the cycles before the 1995 Chile tsunami (blue), coincident with the tsunami (red), and after the tsunami (green). (a) Sea surface height. (b) Ku-band radar backscattering strength

surface roughness are apparent (Fig. 11A). Values shown are computed from equations 1 and 2, assuming a constant background wind of 3 m/ s and a SSH profile derived from the Jason-1 measurements for the 2004 Sumatra-Andaman tsunami (the two-dimensional SSH values were not measured directly by Jason-1, but are representative of the magnitudes during the Sumatra-Andaman tsunami). When using the QuikSCAT wind speeds from December 26, 2004 (the day of the Sumatra-Andaman tsunami), however, the tsunami-induced σ_0 changes are obscured by the variability of the background wind field (Fig. 11B). As in the one-dimensional case, it will likely be necessary to find an appropriate method for
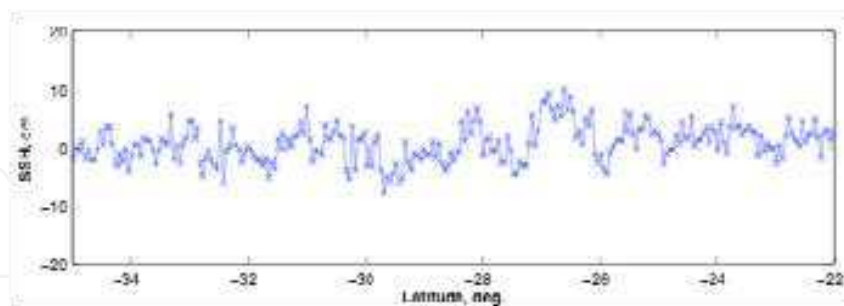

Fig. 10. TOPEX/ Posedion data for pass 232 from 35°S to 22°S filtered using cycles before and after the cycle containing the tsunami. The amplitude of the signal is greatly reduced as a result of the similarity between the three signals, as seen in Fig. 9A

filtering the data to allow separation of the tsunami-induced signal from the background wind variability and measurement noise.

To date, searches of two-dimensional images of ocean surface roughness measurements from instruments already on orbit have not yielded any positive identification of a tsunami-induced signal, partially due to poor sampling coincident with the events. Nevertheless, it is possible that sufficient satellite sampling of the tsunami wavefront and other physical

characteristics of the tsunami could be utilized in the detection of a tsunami using changes in ocean surface roughness. Multiple two-dimensional images of the same region obtained with relatively short time separation could allow for the use of the rapid propagation speed and large spatial extent of the tsunami in the open ocean to aid in the early detection of the tsunami signal. Lognonn

6. Summary and conclusions

Satellite altimeters provide the chance to study the effects of a tsunami wave in the open ocean through concurrent measurements of the sea surface height and the radar backscattering strength. Availability of the SSH data allows one to compare statistical properties of the radar backscattering strength when there is and there is not a tsunami wave present, without having to use tsunami source and propagation models. Using satellite altimeter observations, we have demonstrated that tsunamis in the open ocean cause distinct, measurable changes in ocean surface roughness. We have shown this to be true definitively for the 2004 Sumatra-Andaman tsunami and tentatively true for the 2010 Chile tsunami, 1992 Nicaragua tsunami, and 1995 Chile tsunami.

Although the feasibility of tsunami detection from changes in ocean surface roughness has been demonstrated using measurements from satellite altimeters, the practical issue of optimal retrieval of a tsunami signal from other sources of ocean roughness measurements remains an open question. Use of radar backscattering measurements from satellite altimeters would be impractical for tsunami detection and early warning purposes because of the limited number of operational satellite altimeters. Even if the data could be processed quickly enough to be useful, the temporal resolution and spatial coverage of nadir pointing altimeter measurements is not adequate for tsunami detection and warning. The tsunami-
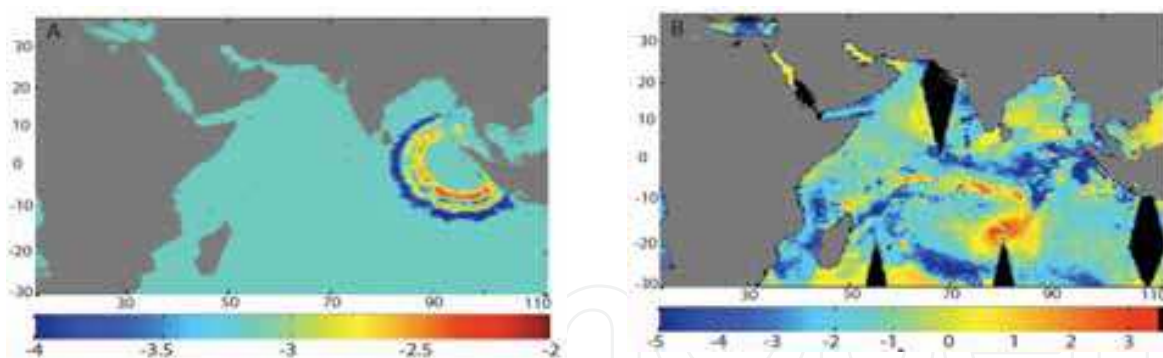

Fig. 11. Using the model presented in Godin et al. (2009) and equations 1 & 2, the two-dimensional field of radar backscattering strength (dB) is computed for A) a constant background wind of 3 m/ s, and B) a background wind field obtained from QUIKSCAT on December 26, 2004. SSH data used for computing the values has been derived from the Jason-1 measurements of the 2004 Sumatra-Andaman tsunami

induced surface roughness variations, however, are likely to be observable with other types of space and airborne sensors. Unlike the sea surface height, which is measured at nadir points along the satellite ground track, variations in ocean surface roughness can potentially be measured over wider swaths with side-looking radars and scanning microwave radiometers. The broader surface coverage of these sensors suggests that they are more promising for early tsunami detection and may be an important component in a future

global system for tsunami detection and warning. Further research is required to demonstrate tsunami detection with such instruments and, as seen in Fig. 9, appropriate analysis techniques will have to be developed to extract the tsunami signal from such data. We anticipate that our study will stimulate the development of data processing algorithms and microwave sensors for the identification of tsunami-induced ocean surface roughness changes to complement or enhance existing regional tsunami detection and early warning systems and contribute to a future global system.

7. References

Ablain, M., Dorandeu, J., Le Traon, P.-Y., and Sladen A., (2006). High resolution altimetry reveals new characteristics of the December 2004 Indian Ocean tsunami, *Geophys. Res. Lett.*, 33, L21602, doi:10.1029/ 2006GL027533.

Artru, J, Lognonné, P., Occhipinti, G., Crespon, F., Garcia, R., Jeansou, E., Murakami, M. (2005). Tsunami detection in the ionosphere, *Space Res. Today*, 163, 23-27.

Behrens, J, Androsov, A., Harig, S., Klaschka, F., Mentrup, L., Pranowo, W. S., Cui, H. Y., Schroter, J, and Hiller, W. (2008). Design and performance testing of a multi-sensor quick assimilation technique for tsunami early warning in the GITEWS simulation system, *Geophys. Res. Abstr.*, 10, EGU2008-A-01878.

Bernard, E. N., Mofjeld, H. O., Titov, V., Synolakis, C. E., and Gonzalez, F. I., (2006). Tsunami: scientific frontiers, mitigation, forecasting and policy implications, *Phil. T. R. Soc. A*, 364, 1989–2007, doi:10.1098/ rsta.2006.1809.

Dudley, W. C. and Lee, M. (1998). Tsunami!, University of Hawaii Press, Honolulu, 5 pp., 302–303, 321–322.

Edgington, E. S. (1995). Randomization Tests, Marcel Dekker, New York.

Fine, I. V., Rabinovich, A. B., and Thomson, R. E. (2005). The dual source region for the 2004 Sumatra tsunami, *Geophys. Res. Lett.*, 32, L16602, doi:10.1029/ 2005GL023521.

Freilich, M. H. and Challenor, P. G. (1995). A new approach for determining fully empirical altimeter wind speed model functions, *J Geophys. Res.*, 99, 25051–25062.

Fujii, Y. and Satake, K. (2007). Tsunami source of the 2004 Sumatra-Andaman earthquake inferred from tide gauge and satellite data, *B. Seismol. Soc. Am.*, 97, 192–207, doi:10.1785/ 0120050613.

Garratt, J. R. (1994). The Atmospheric Boundary Layer, Cambridge University Press, Cambridge.

Geist, E. L., Titov, V. V., Arcas, D., Pollitz, F. F., and Bilek, S. L. (2007). Implications of the 26 December 2004 Sumatra-Andaman earthquake on tsunami forecast and assessment models for great subduction-zone earthquakes, *B. Seismol. Soc. Am.,* 97, 249–270, doi:10.1785/ 0120050619.

Godin, O. A. (2003). Influence of long gravity waves on wind velocity in the near-water layer and feasibility of early tsunami detection, *Dokl. Earth Sci.*, 391, 841–844.

Godin, O. A. (2004). Air-sea interaction and feasibility of tsunami detection in the open ocean, *J Geophys. Res.*, 109, C05002, doi:10.1029/ 2003JC002030.

Godin, O. A. (2005). Wind over fast waves and feasibility of early tsunamidetection from space, in: Frontiers of Nonlinear Physics, edited by: Litvak, A., Inst. Appl. Phys., Nizhny Novgorod, 210–215.

Godin, O. A. and Irisov, V. G. (2003). A perturbation model of radiometric manifestations of oceanic currents, *Radio Sci.*, 38, 8070, doi:10.1029/ 2002RS002642.

Godin, O.A, Irisov, V.G., Leben, R.R., Hamlington, B.D., Wick, G.A. (2009). Variations in sea surface roughness induced by the 2004 Sumatra-Andaman Tsunami, *Nat. Hazards Earth Syst. Sci.*, 9, 1135-1147.

Gonzalez, F. I., Bernard, E. N., Meinig, C., Eble, M. C., Mofjeld, H. O., and Stalin, S. (2005). The NTHMP tsunameter network, *Nat. Hazards*, 35, 25–39, doi: 10.1007/ s11069-004-2402-4.

Gower, J. (2007). The 26 December 2004 tsunami measured by satellite altimetry, *Int. J Remote Sens.*, 28, 2897–2913, doi:10.1080/ 01431160601094484.

Hara, T. and Plant, W. J. (1994). Hydrodynamic modulation of short wind-wave spectra by long waves and its measurement using microwave backscatter, *J Geophys. Res.*, 99, 9767–9784.

Hayashi, Y. (2008). Extracting the 2004 Indian Ocean tsunami signals from sea surface height data observed by satellite altimetry, *J Geophys. Res.*, 113, C01001, doi:10.1029/ 2007JC004177.

Hirata, K., Satake, K., Tanioka, Y., Kuragano, T., Hasegawa, Y., Hayashi, Y., and Hamada, N. (2006). The 2004 Indian Ocean tsunami: Tsunami source model from satellite altimetry, *Earth Planets Space*, 58, 195–201.

Hoechner, A., Babeyko, A. Y., and Sobolev, S. V. (2008). Enhanced GPS inversion technique applied to the 2004 Sumatra earthquake and tsunami, *Geophys. Res. Lett.*, 35, L08310, doi:10.1029/ 2007GL033133.

Kanamori, H. and Kikuchi, M. (1993). The 1992 Nicaragua Earthquake: a slow tsunami earthquake associated with subducted sediments, *Nature*, 361, 714-716.

Kudryavtsev, V. N., Mastenbroek, C., and Makin, V. K. (1997). Modulation of wind ripples by long surface waves via the air flow: a feedback mechanism, *Bound.-Lay. Meteorol.*, 83, 99–116.

Kulikov, E. A., Medvedev, P. P., and Lappo, S. S. (2005). Satellite recording of the Indian Ocean tsunami on December 26, 2004, *Dokl. Earth Sci.*, 401A, 444–448.

Kumar, B. P., Kumar, R. R., Dube, S. K., Murty, T., Gangopadhyay, A., Chaudhuri, A., and Rao A. D. (2006) Tsunami travel time computation and skill assessment for the 26 December 2004 event in the Indian Ocean, *Coast. Eng. J*, 48, 147–166.

Lay, T., Kanamori, H., Ammon, C. J, Nettles, M., Ward, S. N., Aster, R. C., Beck, S. L., Bilek, S. L., Brudzinski, M. R., Butler, R., DeShon, H. R., Ekstrom, G., Satake, K., and Sipkin, S. (2005). The Great Sumatra-Andaman Earthquake of 26 December 2004, Science, 308, 1127–1133, doi:10.1126/ science.1112250.

Lautenbacher, C. C. (2005). Tsunami warning systems, *The Bridge*, 35, 21–25.

Levin, B. W. and Nosov, M. A. (2005). Physics of Tsunamis and Kindred Phenomena, Janus-K, Moscow.

Naeije, M. , Schrama, E., and Scharroo, R. (2000). The Radar Altimeter Database System project RADS. *Proc. of the IEEE 2000 Int. Geoscience and Remote Sensing Symp. (IGARSS 2000),* Honolulu, HI, IEEE, 487-490.

Nagai, T., Kato, T., Moritani, N., Izumi, H., Terada, Y., and Mitsui, M. (2007). Proposal of hybrid tsunami monitoring network system consisted of offshore, coastal and on-site wave sensors, *Coast. Eng. J*, 49, 63–76.

Occhipinti, G., Lognonné, P., Kherani, A., Hebert, H. (2006). 3D Waveform modeling of ionospheric signature induced by the 2004 Sumatra tsunami, *Geophys. Res. Lett.*, doi:10.1029/ 2006GL026865.

Okal, E. A., Piatanesi, A., and Heinrich, P. (1999) Tsunami detection by satellite altimetry, *J Geophys. Res.*, 104, 599–615.

Powell, B. S. and Leben, R. R. (2004) An optimal filter for geostrophic mesoscale currents from along-track satellite altimetry, *J. Atmos. Ocean. Tech.,* 21, 1633–1642.

Rowan, L. (2004). Tsunami and its shadow, *Science*, 304, p.1569.

Schindele, F., Loevenbruck, A., and Hebert, H. (2008). Strategy to design the sea-level monitoring networks for small tsunamigenic oceanic basins: the Western Mediterranean case, *Nat. Hazards Earth Syst. Sci.*, 8, 1019–1027, http://www.nat-hazards-earth-syst-sci.net/8/1019/2008/.

Sladen, A. and Hebert, H. (2008) On the use of satellite altimetry to infer the earthquake rupture characteristics: application to the 2004 Sumatra event, *Geophys. J. Int.*, 172, 707–714, doi:10.1111/j.1365-246X.2007.03669.x.

Smith, W. H. F., Scharroo, R., Titov, V. V., Arcas, D., and Arbic, B. K. (2005) Satellite altimeters measure tsunami, *Oceanography*, 18, 11–13.

Song, T. Y., Ji, C., Fu, L.-L., Zlotnicki, V., Shum, C. K., Yi, Y., and Hjorleifsdottir, V. (2005) The 26 December 2004 tsunami source estimated from satellite radar altimetry and seismic waves, *Geophys. Res. Lett.*, 32, L20601, doi:10.1029/2005GL023683.

Stein, S. and Okal, E. A. (2005) Speed and size of the Sumatra earthquake, *Nature*, 434, 581–582, doi:10.1038/434581a.

Synolakis, C. E. and Bernard, E. N. (2006). Tsunami science before and beyond Boxing Day 2004, *Philos. T. Roy. Soc. A.*, 364, 2231–2265, doi:10.1098/rsta.2006.1824.

Synolakis, C. E., Bernard, E. N., Titov, V. V., Konoglu, U., Gonzalez, F. I. (2008). Validation and verification of tsunami numerical models, *Pure Appl. Geophys.,* 165(11-12), 2197-2228.

Titov, V., Rabinovich, A. B., Mofjeld, H. O., Thomson, R. E., and Gonzalez, F. I. (2005). The global reach of the 26 December 2004 Sumatra tsunami, *Science*, 309, 2045–2048, doi:10.1126/science/1114576.

Troitskaya, Y. I. (1994). Modulation of the growth rate of short surface capillary-gravity wind waves by a long wave, *J. Fluid Mech.*, 273, 169–187.

Troitskaya, Y. I. and Ermakov, S. A. (2005). Recording of the December 26, 2004 tsunami in the open ocean based on variations in radar scattering section, *Dokl. Earth Sci.*, 405A, 1384–1387.

Troitskaya, Y. I. and Ermakov, S. A. (2008) Manifestations of the Indian Ocean tsunami of 2004 in satellite nadir-viewing radar backscattering variations, *Int. J. Remote Sens.*, 29, 6361–6371, doi:10.1080/01431160802175348.

Walker, D. A. (1996). Observations of tsunami "shadows": A new technique for assessing tsunami wave heights?, *Science of Tsunami Hazards*, 14, 3–11.

Wei, Y., Bernard, E. N., Tang, L., Weiss, R., Titov, V. V., Moore, C., Spillane, M., Hopkins, M., and Kanoglu, U. (2008). Realtime experimental forecast of the Peruvian tsunami of August 2007 for US coastlines, *Geophys. Res. Lett.*, 35, L04609, doi:10.1029/2007GL032250.

Witter, D. L. and Chelton, D. B. (1991). A geosat altimeter wind speed algorithm and a method for altimeter wind speed algorithm development, *J. Geophys. Res.*, 96, 8853–8860.

Zaichenko, M. Y., Kulikov, E. A., Levin, B. V., and Medvedev, P. P. (2005). On the possibility of registration of tsunami waves in the open ocean with the use of a satellite altimeter, *Oceanology*, 45, 194–201.

The Tsunami Threat - Research and Technology

Edited by Nils-Axel MÃ¶rner

Submarine earthquakes, submarine slides and impacts may set large water volumes in motion characterized by very long wavelengths and a very high speed of lateral displacement, when reaching shallower water the wave breaks in over land - often with disastrous effects. This natural phenomenon is known as a tsunami event. By December 26, 2004, an event in the Indian Ocean, this word suddenly became known to the public. The effects were indeed disastrous and 227,898 people were killed. Tsunami events are a natural part of the Earth's geophysical system. There have been numerous events in the past and they will continue to be a threat to humanity; even more so today, when the coastal zone is occupied by so much more human activity and many more people. Therefore, tsunamis pose a very serious threat to humanity. The only way for us to face this threat is by increased knowledge so that we can meet future events by efficient warning systems and aid organizations. This book offers extensive and new information on tsunamis; their origin, history, effects, monitoring, hazards assessment and proposed handling with respect to precaution. Only through knowledge do we know how to behave in a wise manner. This book should be a well of tsunami knowledge for a long time, we hope.

How to reference

In order to correctly reference this scholarly work, feel free to copy and paste the following:

Benjamin D. Hamlington, Oleg A. Godin, Vladimir G. Irisov and Robert R. Leben (2011). Detection of Tsunamis from Changes in Ocean Surface Roughness, The Tsunami Threat - Research and Technology, Nils-Axel MÃ¶rner (Ed.), ISBN: 978-953-307-552-5, InTech, Available from: http://www.intechopen.com/books/the-tsunami-threat-research-and-technology/detection-of-tsunamis-from-changes-in-ocean-surface-roughness

INTECH
open science | open minds